Perturbation study of nonequilibrium quasiparticle spectra in an infinite-dimensional Hubbard lattice

R. J. Heary and J. E. Han
Department of Physics, State University of New York at Buffalo, Buffalo, New York 14260, USA
(Received 4 March 2009; revised manuscript received 11 June 2009; published 1 July 2009)

A model for nonequilibrium dynamical mean-field theory is constructed for the infinite-dimensional Hubbard lattice. We impose nonequilibrium by expressing the physical orbital as a superposition of a left (L)-moving and right (R)-moving electronic state with the respective chemical potentials μ_L and μ_R. Using the second-order iterative perturbation theory we calculate the quasiparticle properties as a function of the chemical potential bias between the L and R movers, i.e., $\Phi=\mu_L-\mu_R$. The evolution of the nonequilibrium quasiparticle spectrum is mapped out as a function of the bias and temperature. The quasiparticle states with the renormalized Fermi-energy scale ε_{QP}^0 disappear at $\Phi\sim\varepsilon_{QP}^0$ in the low-temperature limit. The second-order perturbation theory predicts that in the vicinity of the Mott-insulator transition at the Coulomb-parameter $U=U_c$, there exists another critical Coulomb-parameter U_d ($<U_c$) such that, for $U_d<U<U_c$, quasiparticle states are destroyed abruptly when $(\varepsilon_{QP}^0)^2\sim a(\pi k_B T_c)^2+b\Phi_c^2$ with the critical temperature T_c, the critical bias Φ_c, and the numerical constants a and b on the order of unity.

DOI: 10.1103/PhysRevB.80.035102 PACS number(s): 71.10.Fd, 71.30.+h, 73.40.Jn

In recent years significant experimental progress has been made in the fabrication of sophisticated electronic heterostructures utilizing strongly correlated electronic materials. These systems have given rise to the discovery of rich novel phenomena. These include: ballistic transport of electrons through heterostructures of superconductors,[1] ferromagnets,[2] magnetic tunneling junctions,[3,4] and oxides.[5–8] With this vast array of strongly correlated heterostructures it is very important to theoretically understand how the strongly correlated materials in the bulk limit will behave under nonequilibrium conditions. In this work we formulate the nonequilibrium problem in the lattice and present significant progress toward a more complete understanding of strongly correlated lattices out of equilibrium.

We are interested in heterostructures of strongly correlated materials under a finite source-drain bias where the voltage drop occurs mainly at the interface of the strongly correlated material and the source/drain leads, as considered previously.[9,10] By this construction this model may not be sufficient to describe nonequilibrium in true-bulk systems. However, we speculate that this model is relevant to nanoscale devices where the nonequilibrium is established by unequal statistics between ballistic electrons from source and drain. This study will give an insight on how the lattice effects manifest in such systems. Our focus here is to investigate the evolution of strongly correlated quasiparticle spectra due to nonequilibrium driven by an imbalance in the chemical potentials. In this work we gain qualitative understanding on how the enhanced dephasing by the new particle-hole decay channel due to nonequilibrium modifies the spectral properties.

One of the most practical and powerful theoretical techniques for studying strongly correlated lattices is the dynamical mean-field theory (DMFT).[11] Within this approach the self-energy of the strongly correlated lattice becomes momentum independent and as a result the problem is reduced to solving a self-consistent interacting impurity model. This inherent simplicity of DMFT makes it a very attractive tool, especially with the large quantity of exact and perturbative impurity solvers such as the Hirsch-Fye quantum Monte-Carlo method,[12] the numerical renormalization group,[13] and the noncrossing approximation.[14,15]

As an extension of DMFT to nonequilibrium situations, Okamoto has theoretically studied the nonlinear transport and spectral properties of metal-Mott insulator-metal heterostructures where a bias voltage is applied across the Mott insulator[9,10] using layered DMFT.[16] There he combined the layered DMFT technique with the Keldysh Green's-function approach and invoked the noncrossing approximation as the impurity solver. Another system recently studied is the DMFT limit of the Hubbard model with the nonequilibrium driven by a uniform high electric field.[17] Others have looked at the DMFT limit of the Falicov-Kimball model in the presence of a uniform time-dependent electric field and examined the transient current, quenching of the Bloch oscillations, and evolution of the spectral function.[18,19]

In our analysis of the problem we choose to start from the metallic state and analyze how the Fermi liquid is renormalized and eventually destroyed with multiple chemical potentials. We find that the quasiparticles strongly depend upon the strength of the chemical potential difference Φ. At zero Φ it has long been known that the system undergoes a metal-insulator transition at $U=U_c$.[11] The second-order iterative perturbation-theory (IPT) approximation gives $U_c=U_{c2}\simeq 3.3D$ at zero temperature, where D is the half bandwidth. As the temperature is raised the transition remains distinct down to $U_{c1}\simeq 2.6D$. In nonequilibrium, the second-order IPT shows that the quasiparticles are destroyed abruptly by the chemical potential bias in the region $U_d<U<U_c$, where $U_d\simeq 2.3D$. When $U<U_d$ the system exhibits a smooth crossover from a system of well-defined quasiparticle states to that without quasiparticle excitations.

The system of focus is a nonequilibrium system with unequal momentum distribution. For instance, in heterostructure junctions, electrons coming from the source lead with momentum in the transport direction (left movers with k_x

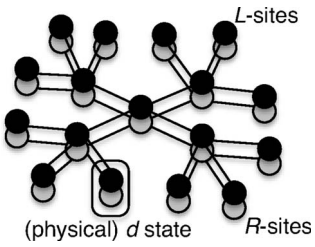

FIG. 1. The Bethe lattice where the (physical) d state is given as a superposition of a left (L)- and a right (R)- moving state with the corresponding chemical potentials $\mu_L=\Phi/2$ and $\mu_R=-\Phi/2$.

>0) have higher density than those from the drain (left movers with $k_x<0$). The site-orbital basis is a superposition of the left and right movers, with the explicit construction given by a dispersion relation on a given lattice structure. Calculation of transport relation, such as current, requires explicit constructions of site orbitals in terms of left and right movers. However, in this work, we only concentrate on the on-site spectral properties and such an explicit construction is not necessary.

Therefore, for simplicity and convenient comparison with the equilibrium DMFT literature, we start with a noninteracting d-dimensional tight-binding Bethe lattice. The tight-binding solutions are grouped evenly into left (L) and right (R) movers with chemical potentials $\mu_L=\Phi/2$ and $\mu_R=-\Phi/2$, respectively. Since we do not study transport properties in this work, it is not important how the physical site is decomposed into L,R movers. The original site orbital $d^\dagger_{i\sigma}$ at site i with spin σ is written as a superposition of L- and R-orbitals $d^\dagger_{L/R,i\sigma}$ according to

$$d^\dagger_{i\sigma}=\frac{1}{\sqrt{2}}(d^\dagger_{L,i\sigma}+d^\dagger_{R,i\sigma}). \tag{1}$$

The interaction terms and any observable quantities ought to be given in the physical basis $d^\dagger_{i\sigma}$. The nonequilibrium DMFT lattice is depicted in Fig. 1.

The model with which we focus is the DMFT limit ($d\to\infty$) of the Hubbard-model $\hat{\mathcal{H}}=\hat{\mathcal{H}}_0+\hat{\mathcal{V}}$,

$$\hat{\mathcal{H}}_0=-t_0\sum_{\langle i,j\rangle}\sum_{\alpha=L,R;\sigma}(d^\dagger_{\alpha,i\sigma}d_{\alpha,j\sigma}+\text{h.c.}), \tag{2}$$

$$\hat{\mathcal{V}}=U\sum_i\left(d^\dagger_{i\uparrow}d_{i\uparrow}-\frac{1}{2}\right)\left(d^\dagger_{i\downarrow}d_{i\downarrow}-\frac{1}{2}\right). \tag{3}$$

The noninteracting tight-binding part of the Hamiltonian $\hat{\mathcal{H}}_0$ takes into account the hopping of electrons between nearest-neighbor lattice sites of the Bethe lattice with the tight-binding parameter t_0. The interaction term of the Hamiltonian $\hat{\mathcal{V}}$ is the particle-hole symmetric on-site Coulomb interaction of strength U. Both the noninteracting and interacting terms of the Hamiltonian are homogeneous in real space, which is necessary for our application of single-site DMFT. The Hamiltonian may be further simplified by transforming the L and R basis into the even (E) and odd (O) superposition of the basis. The creation operators for the even and odd electron orbitals are $d^\dagger_{E/O,i\sigma}=(d^\dagger_{L,i\sigma}\pm d^\dagger_{R,i\sigma})/\sqrt{2}$. The interaction is only given by the even (physical) basis and the noninteracting part is decoupled into the even-odd parts as $\hat{\mathcal{H}}_0=-t_0\Sigma_{\langle i,j\rangle}\Sigma_{\alpha=E,I;\sigma}(d^\dagger_{\alpha,i\sigma}d_{\alpha,j\sigma}+\text{h.c.})$. Therefore, the time evolution of even (physical) and odd states are completely decoupled and the perturbation theory of DMFT is applied within the physical basis where the nonequilibrium statistics are imposed on the noninteracting Green's functions.

This Hamiltonian is solved using the iterative perturbation theory.[11] The IPT has been extensively utilized and well-established in equilibrium DMFT and we anticipate that the second-order IPT gives a qualitatively reasonable description of the quasiparticle destruction in nonequilibrium. However we caution that the second-order perturbation theory may not capture the exact nature of the quasiparticles in nonequilibrium. For example, it is known that second-order perturbation theory does not properly describe the splitting of the Kondo peak in quantum-dot devices with a finite voltage bias, as seen in the fourth-order perturbation theory[20] and in nonperturbative solvers.[21,22] Therefore, it still remains to be seen through nonperturbative calculations which of the following results will hold up.

Now we outline the DMFT self-consistent routine. The calculation is performed in real time as opposed to real frequency because close to the Mott-insulator transition the bath spectral function becomes sharply peaked at the Fermi energy,[23] thus making the real frequency calculation very difficult. In the noninteracting limit the (even) bath Green's function is given by

$$\begin{bmatrix} g^<(t) \\ g^>(t) \end{bmatrix}=\frac{i}{2}\sum_{\alpha=L,R}\int d\epsilon D(\epsilon)\begin{bmatrix} f_\alpha(\epsilon) \\ f_\alpha(\epsilon)-1 \end{bmatrix}e^{-i\epsilon t}, \tag{4}$$

where $f_L(\epsilon)=f(\epsilon-\frac{\Phi}{2})$ and $f_R(\epsilon)=f(\epsilon+\frac{\Phi}{2})$ are the Fermi functions for the L and R movers. $D(\epsilon)$ is the noninteracting density of states (DOS), which we have taken to be semicircular $D(\epsilon)=\frac{2}{\pi D^2}\sqrt{D^2-\epsilon^2}$. In the following, $D=1$ is used as the unit of energy. A typical time bandwidth we use is $\sim 3000D^{-1}$ which corresponds to the energy scale of $10^{-4}D$.

Within IPT the self-energy is calculated to second order in U. Using the Langreth theorem[24] we may calculate the lesser and greater self-energies according to

$$\Sigma^{\gtrless}_{\text{int}}(t)=U^2[g^{\gtrless}(t)]^2g^{\lessgtr}(-t). \tag{5}$$

The lesser and greater self-energies are then Fourier transformed to real frequency. The lesser (greater) self-energy gives us the particle (hole) spectral weight as a function of frequency for the retarded self-energy. Using the Keldysh Green's-function relation $\Sigma^r_{\text{int}}(\omega)-\Sigma^a_{\text{int}}(\omega)=\Sigma^>_{\text{int}}(\omega)-\Sigma^<_{\text{int}}(\omega)$, we may express the retarded self-energy in the spectral form

$$\Sigma^r_{\text{int}}(\omega)=\frac{1}{2\pi}\int d\epsilon\frac{\text{Im}[\Sigma^<_{\text{int}}(\epsilon)-\Sigma^>_{\text{int}}(\epsilon)]}{\omega-\epsilon+i\eta}. \tag{6}$$

The nonequilibrium DMFT self-consistent equations for the interacting and bath Green's function are therefore

$$G^r(\omega)=\int d\epsilon\frac{D(\epsilon)}{\omega-\epsilon-\Sigma^r_{\text{int}}(\omega)}, \tag{7}$$

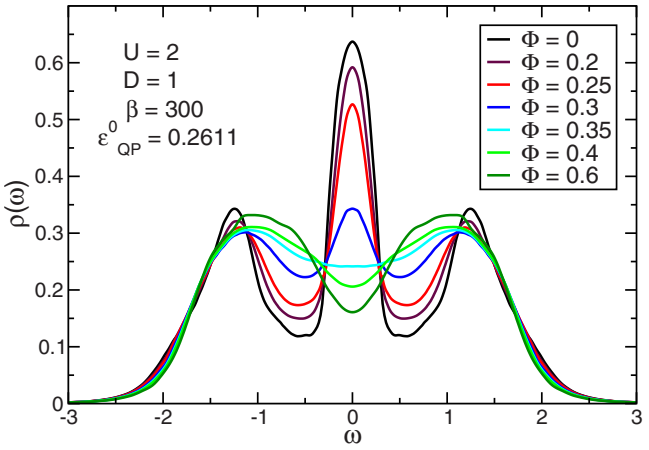

FIG. 2. (Color online) Interacting local spectral functions for $U=2$, inverse temperature $\beta=300$ and half-bandwidth $D=1$ plotted for a range of chemical potential biases, Φ. At this value of the Coulomb-interaction U the quasiparticle peak is destroyed continuously as Φ is increased.

$$g^r(\omega)^{-1} = \omega + i\eta - t^2 G^r(\omega), \tag{8}$$

where $\rho_0(\omega) = -\pi^{-1}\,\mathrm{Im}[g^r(\omega)]$ is the new bath DOS. For the new Keldysh bath Green's functions we replace the noninteracting DOS in Eq. (4) with $\rho_0(\omega)$. The momentum independence of the self-energy and the translational invariance ensure that the wave vectors remain good quantum numbers. We iterate these equations until the bath Green's function and interacting Green's function converge.

From previous works in the equilibrium system,[11] it is known that by increasing the temperature the quasiparticles are destroyed when the thermal fluctuations surpass a certain low-energy scale. This low-energy scale is given by the renormalized Fermi-energy ε_{QP} which we define as the half width at half maximum (HWHM) of the quasiparticle peak and is similar to $\epsilon_F^* = ZD$ where $Z = \{1 - \partial_\omega\,\mathrm{Re}[\Sigma^r(\omega)]\big|_{\omega=0}\}^{-1}$ is the quasiparticle weight, as found in Georges *et al.*[11] As the temperature is increased at zero-bias $\Phi=0$, the quasiparticles are destroyed when $k_B T_c \sim \varepsilon_{QP}^0$ where T_c is the critical temperature. ε_{QP}^0 is the quasiparticle half bandwidth at zero bias.

Figures 2–4 show the evolution of quasiparticle spectra as a function of bias Φ. The destruction of the Fermi liquid is easily understood by enhanced dephasing of particles and holes, which is a consequence of the opening up of phase space available for the particles/holes to scatter into through Φ and by thermal fluctuations. Both of these effects lead to a finite lifetime for the electron at the Fermi energy. To lowest order in ω, T, and Φ the imaginary part of the self-energy obeys the relation[25]

$$\lim_{\omega,T,\Phi\to 0} \mathrm{Im}[\Sigma^r(\omega)] \propto \left[\omega^2 + (\pi k_B T)^2 + \frac{3}{4}\Phi^2\right]. \tag{9}$$

The interacting spectral-function $\rho(\omega)$ is calculated both as a function of the Coulomb-interaction U and the applied chemical potential bias Φ. For $U < U_d$ with $U_d \simeq 2.3D$, the destruction of the quasiparticle peak is continuous, and exhibits similar behavior to the metal-insulator transition in the crossover regime ($U < U_{c1}$) of equilibrium DMFT. Our results at $U = 2D (< U_d)$ are shown in Fig. 2. As the chemical potential bias is increased the quasiparticle weight smoothly shifts toward the upper and lower Hubbard bands, and the quasiparticle peak disappears when $\Phi \sim \varepsilon_{QP}^0$.

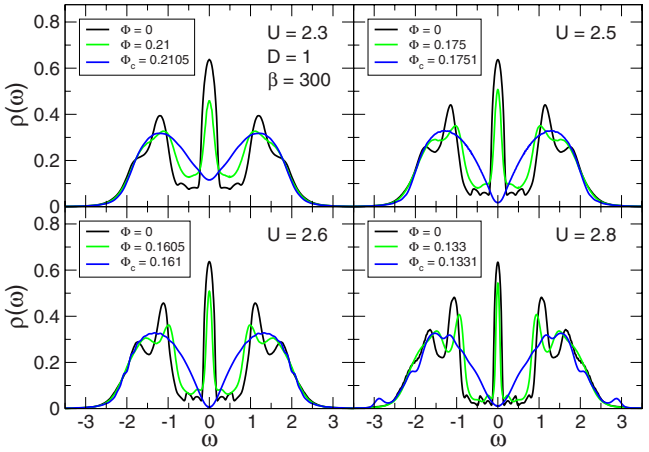

FIG. 3. (Color online) Interacting local spectral functions for $U=2.3$, 2.5, 2.6, and 2.8 at inverse temperature $\beta=300$ and bandwidth $D=1$. These plots depict the sudden disappearance of the quasiparticle peak at the critical voltage Φ_c. The spectral functions are plotted at $\Phi=0$, at Φ just before the quasiparticle destruction, and at $\Phi=\Phi_c$.

For $U_d < U < U_c$ the quasiparticle peak is discontinuously destroyed at a critical chemical potential bias Φ_c. In Fig. 3 we have plotted the interacting spectral functions for $U/D = 2.3$, 2.5, 2.6, and 2.8 to illustrate the sudden disappearance of the quasiparticle peak. The spectral function for each value of U is shown for $\Phi=0$, Φ just before the transition, and finally at the transition $\Phi=\Phi_c$. This discontinuous transition in nonequilibrium by bias is reminiscent of the discontinuous transition by temperature in the equilibrium DMFT.

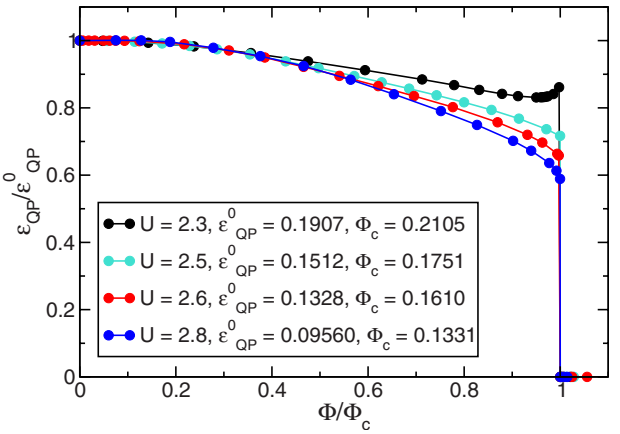

FIG. 4. (Color online) Quasiparticle-energy ε_{QP} as a function of the chemical potential bias Φ at $\beta=300$ and $D=1$. The quasiparticle energy is scaled to the quasiparticle energy at zero bias, ε_{QP}^0, and the chemical potential bias is scaled to the critical bias at which the quasiparticle peak is destroyed, Φ_c. For small bias, $\Phi \lesssim 0.4\Phi_c$, the quasiparticle energies scale to a single curve. In this range of values for U the disappearance of the quasiparticle peak is strongly discontinuous.

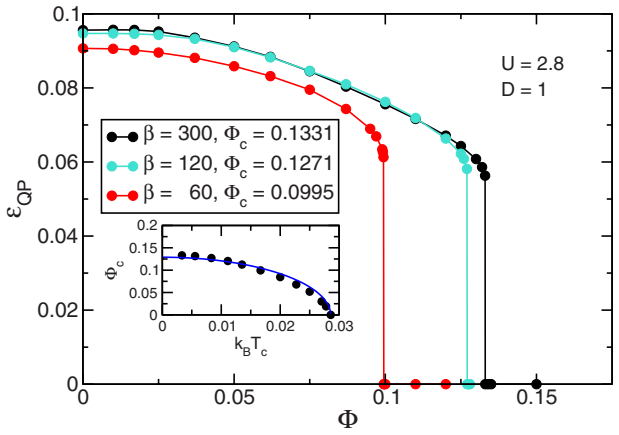

FIG. 5. (Color online) Quasiparticle-energy ε_{QP} as a function of the chemical potential bias Φ at $U=2.8$ and $D=1$ for different values of the inverse temperature β. As the temperature is increased, the disappearance of quasiparticles remains discontinuous and the critical bias Φ_c is lowered. The inset gives the temperature dependence of the critical bias. The data (filled circles) were fit (solid curve) to the function, $(\varepsilon^0_{QP})^2 \sim a(\pi k_B T_c)^2 + b\Phi_c^2$, where $a=1.1$ and $b=0.54$.

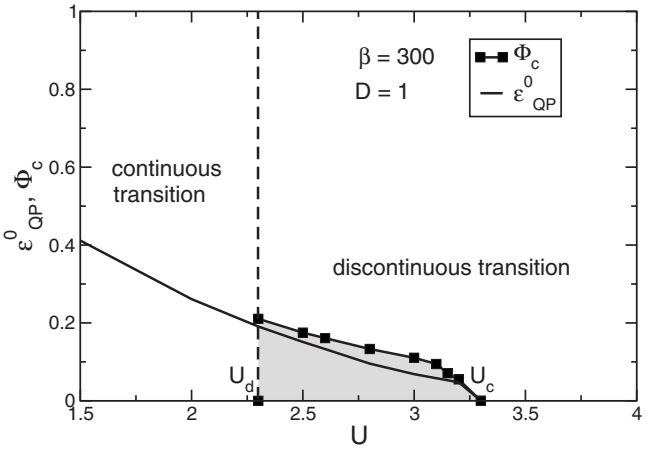

FIG. 6. The critical bias Φ_c is plotted as a function of the Coulomb-interaction U at inverse temperature $\beta=300$ and bandwidth $D=1$. We have also plotted the renormalized Fermi-energy ε^0_{QP} at $\Phi=0$. In the region $U_d<U<U_c$ the quasiparticle peak is destroyed discontinuously at Φ_c. When $U<U_d$ the quasiparticle peak disappears smoothly with increasing chemical potential bias. At this temperature $\Phi_c \sim \varepsilon^0_{QP}$.

In Fig. 4 the scaled quasiparticle-energy $\varepsilon_{QP}/\varepsilon^0_{QP}$ is plotted versus the scaled chemical potential bias Φ/Φ_c. For $\Phi \lesssim 0.4\Phi_c$ the curves for $U/D=2.3$, 2.5, 2.6, and 2.8 scale onto a single curve. At $\Phi=\Phi_c$ it is clearly visible that the quasiparticle peak disappears discontinuously for each value of U.

In Fig. 5 we take a closer look at the temperature dependence of the transition in the discontinuous region. At $U=2.8$, which is well into this region, the quasiparticle disappearance remains discontinuous for the entire range of temperatures. Therefore the discontinuous nature of the transition is very robust and is not effected by the temperature. The inset yields the dependence of the critical bias upon temperature. Motivated by the form of the imaginary part of the self-energy [Eq. (9)], we anticipate that the destruction of the quasiparticles will occur when $(\varepsilon^0_{QP})^2 \sim a(\pi k_B T_c)^2 + b\Phi_c^2$ at critical values for the temperature T_c and the bias Φ_c. In Fig. 5 we fit Φ_c versus T_c to this function and find that $a=1.1$ and $b=0.54$. Considering the nonlinear effects in the numerical results, the obtained values a and b are in reasonable agreement with the estimates 1 and $\frac{3}{4}$ based on Eq. (9).

The critical bias Φ_c and renormalized Fermi-energy ε^0_{QP} are plotted versus U in Fig. 6 at $\beta=300$. The onset of the discontinuous transition is marked at $U_d \simeq 2.3D$ and the Mott-insulator transition at $\Phi=0$ is given at $U_c \simeq 3.3D$. We see that the transition occurs at $\Phi_c \sim \varepsilon^0_{QP}$ which further justifies the function used for fitting Φ_c versus $k_B T_c$ of Fig. 5.

In this work we have presented a theoretical model for nonequilibrium dynamical mean-field theory and performed the iterative perturbation calculations within the dynamical mean-field theory. In a lattice where the statistics are determined by the presence of multiple chemical potentials, the quasiparticle properties are strongly dependent upon the strength of the Coulomb interaction and the chemical potential bias, Φ. For $U<U_d$ with $U_d \simeq 2.3D$ for the bandwidth D, the quasiparticle disappears smoothly with increasing chemical potential bias. The disappearance of the quasiparticles is caused by the opening up of phase space for the electrons to scatter into at the Fermi energy, resulting in a finite lifetime for the electrons. The perturbation theory also predicts that in the region $U_d<U<U_c$, where $U_c \simeq 3.3D$ marks the Mott-insulator transition in equilibrium, the quasiparticle particles may be destroyed discontinuously at a critical bias, Φ_c.

This work was supported by NSF (Grant No. DMR-0426826) and we acknowledge the CCR at SUNY Buffalo for computational resources.

[1] G. Bastian, E. O. Göbel, A. B. Zorin, H. Schulze, J. Niemeyer, T. Weimann, M. R. Bennett, and K. E. Singer, Phys. Rev. Lett. **81**, 1686 (1998).

[2] J. Salafranca, M. J. Calderón, and L. Brey, Phys. Rev. B **77**, 014441 (2008).

[3] J. M. De Teresa, A. Barthélémy, A. Fert, J. Contour, F. Montaigne, and P. Seneor, Science **286**, 507 (1999).

[4] M. R. McCartney, R. E. Dunin-Borkowski, M. R. Scheinfein, D. J. Smith, S. Gider, and S. Parkin, Science **286**, 1337 (1999).

[5] S. Thiel, G. Hammerl, A. Schmehl, C. W. Schneider, and J. Mannhart, Science **313**, 1942 (2006).

[6] J. Chakhalian, J. W. Freeland, G. Srajer, J. Strempfer, G. Khaliullin, J. C. Cezar, T. Charlton, R. Dalgliesh, C. Bernhard, G. Cristiani, H.-U. Habermeier, and B. Keimer, Nat. Phys. **2**, 244 (2006).

[7] A. Brinkman, M. Huijben, M. van Zalk, J. Huijben, U. Zeitler, J.

C. Maan, W. G. van der Wiel, G. Rijnders, D. H. A. Blank, and H. Hilgenkamp, Nature Mater. **6**, 493 (2007).
[8] N. Reyren, S. Thiel, A. D. Caviglia, L. F. Kourkoutis, G. Hammerl, C. Richter, C. W. Schneider, T. Kopp, A.-S. Rüetschi, D. Jaccard, M. Gabay, D. A. Muller, J.-M. Triscone, and J. Mannhart, Science **317**, 1196 (2007).
[9] S. Okamoto, Phys. Rev. B **76**, 035105 (2007).
[10] S. Okamoto, Phys. Rev. Lett. **101**, 116807 (2008).
[11] A. Georges, G. Kotliar, W. Krauth, and M. J. Rozenberg, Rev. Mod. Phys. **68**, 13 (1996).
[12] J. E. Hirsch and R. M. Fye, Phys. Rev. Lett. **56**, 2521 (1986).
[13] H. R. Krishna-murthy, J. W. Wilkins, and K. G. Wilson, Phys. Rev. B **21**, 1003 (1980); Phys. Rev. B **21**, 1044 (1980).
[14] Th. Pruschke and N. Grewe, Z. Phys. B: Condens. Matter **74**, 439 (1989).
[15] T. Pruschke, D. L. Cox, and M. Jarrell, Phys. Rev. B **47**, 3553 (1993).
[16] S. Okamoto and A. J. Millis, Phys. Rev. B **70**, 241104(R) (2004).
[17] A. V. Joura, J. K. Freericks, and Th. Pruschke, Phys. Rev. Lett. **101**, 196401 (2008).
[18] J. K. Freericks, V. M. Turkowski, and V. Zlatic, Phys. Rev. Lett. **97**, 266408 (2006).
[19] J. K. Freericks, Phys. Rev. B **77**, 075109 (2008).
[20] T. Fujii and K. Ueda, Phys. Rev. B **68**, 155310 (2003).
[21] J. E. Han and R. J. Heary, Phys. Rev. Lett. **99**, 236808 (2007).
[22] F. B. Anders, Phys. Rev. Lett. **101**, 066804 (2008).
[23] X. Y. Zhang, M. J. Rozenberg, and G. Kotliar, Phys. Rev. Lett. **70**, 1666 (1993).
[24] D. C. Langreth, in *Linear and Nonlinear Electron Transport in Solids*, edited by J. T. Devreese and V. E. Doren, NATO Advanced Studies Institute, Series B: Physics (Plenum, New York, 1976), Vol. 17.
[25] A. Oguri, Phys. Rev. B **64**, 153305 (2001).